

Conformal Boundary Conditions of Symmetry-Enriched Quantum Critical Spin Chains

Xue-Jia Yu,^{1,*} Rui-Zhen Huang,^{2,*} Hong-Hao Song,² Limei Xu,^{1,3,4} Chengxiang Ding,⁵ and Long Zhang^{2,†}

¹International Center for Quantum Materials, School of Physics, Peking University, Beijing 100871, China

²Kavli Institute for Theoretical Sciences and CAS Center for Excellence in Topological Quantum Computation, University of Chinese Academy of Sciences, Beijing, 100190, China

³Collaborative Innovation Center of Quantum Matter, Beijing, China

⁴Interdisciplinary Institute of Light-Element Quantum Materials and Research Center for Light-Element Advanced Materials, Peking University, Beijing, China

⁵School of Science and Engineering of Mathematics and Physics, Anhui University of Technology, Maanshan, Anhui 243002, China

(Dated: November 23, 2021)

Some quantum critical states cannot be smoothly deformed into each other without explicitly breaking certain symmetries even if they belong to the same universality class. This brings up the notion of “symmetry-enriched” quantum criticality. In this work, we propose that the conformal boundary condition (b.c.) is a more generic characteristic of such quantum critical states than the robust edge degeneracy studied recently. We show that in two families of quantum spin chains, which generalize the Ising and the three-state Potts models, the quantum critical point between a symmetry-protected topological phase and a symmetry-breaking order realizes a conformal b.c. distinct from the simple Ising and Potts chains. Furthermore, we argue that the conformal b.c. can be derived from the bulk effective field theory, which constitutes a novel bulk-boundary correspondence in symmetry-enriched quantum critical states.

Introduction.—The development of topological states of matter has greatly deepened our understanding of gapped phases [1]. For example, one-dimensional (1D) symmetry-protected topological (SPT) states are fully classified by the projective representations of the symmetry group and host degenerate edge modes, which transform as the projective representations [2, 3]. Different SPT phases cannot be adiabatically connected without explicitly breaking the symmetry.

Quantum critical states enjoy the scale invariance in the low-energy limit, and fall into different universality classes characterized by the operator scaling dimensions. Surprisingly, some quantum critical states cannot be smoothly connected despite that they belong to the same universality class. This brings up the notion of gapless SPT [4, 5] or “symmetry-enriched” quantum critical states [6]. Robust degenerate edge states persist in some quantum critical states [4–20], which are secured by the symmetry-flux (disorder) operators in the bulk carrying nontrivial symmetry charges [6]. This signifies a novel bulk-boundary correspondence. However, a signature of symmetry-enriched quantum critical states without edge degeneracy is still lacking.

In this work, we shall show that the conformal boundary condition (b.c.) and the associated surface critical behavior are more generic characteristics of symmetry-enriched quantum criticality. For a critical system with boundary, a conformal b.c. corresponds to a fixed point of the renormalization group (RG) flow of the boundary states. Different conformal b.c. can be specified for a given conformal field theory (CFT) in the bulk, resulting into rich surface critical phenomena.

The conformal b.c. determines the operator content of the system [21, 22], i.e., the Hamiltonian eigenstates, which are organized into conformal families, each comprising a primary state and all its conformal descendants. The conformal b.c. also determines the universality of the surface criticality [21, 23]. Given a local operator on the boundary [denoted by $\phi(r)$] and in the bulk [$\phi_b(R)$], the following connected correlation functions scale as

$$C_{\parallel}(r_1 - r_2) = \langle \phi(r_1)\phi(r_2) \rangle_c \propto |r_1 - r_2|^{-2\Delta_{\phi}}, \quad (1)$$

$$C_{\perp}(r - R) = \langle \phi(r)\phi_b(R) \rangle_c \propto |r - R|^{-\Delta_{\phi} - \Delta_{\phi}^b}, \quad (2)$$

in which $\langle AB \rangle_c = \langle AB \rangle - \langle A \rangle \langle B \rangle$. $r_1 - r_2$ is parallel to the surface, while $r - R$ is perpendicular to it. Δ_{ϕ} and Δ_{ϕ}^b are the scaling dimensions of the boundary and the bulk operators, respectively. The surface critical behavior of classical statistical systems has been extensively studied [24, 25]. The interest in the surface criticality has been revived recently partly motivated by the fate of topological edge states at quantum critical points (QCPs), leading to the discovery of new surface universality classes [26–39].

In this work, we study two families of quantum spin chains, which generalize the 1D Ising and the three-state Potts models [17, 18, 40], respectively. Each family contains quantum critical states that are described by the same CFT but cannot be smoothly connected. While the two Ising QCPs can be distinguished by the edge modes [6, 17, 18], the generalized Potts chain lacks such a distinctive feature. By examining their surface critical behavior and the energy and entanglement spectra, we show that in each family of models, the QCP between an SPT and a symmetry-breaking order realizes a conformal b.c. distinct from the simple Ising and Potts models.

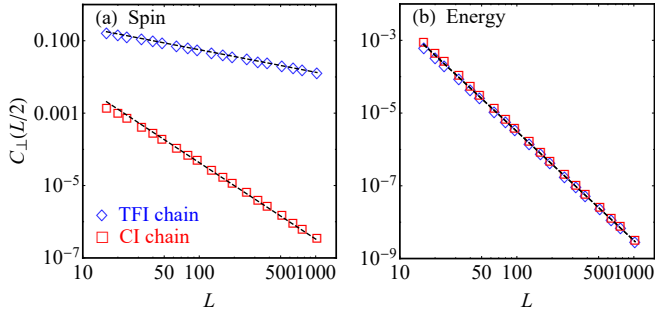


FIG. 1. Connected correlation functions $C_{\perp}(L/2)$ of (a) the spin operator σ_l^z and (b) the energy operator $\epsilon_l = \sigma_l^z \sigma_{l+1}^z$ in the critical Ising chains. Dashed lines are the power-law fitting according to Eq. (2).

Moreover, the conformal b.c. can be derived from the effective field theory of the bulk states, thus establishing a novel bulk-boundary correspondence in symmetry-enriched quantum critical states.

Warm-up: Quantum Ising chains.—We first study the following transverse-field Ising (TFI) chain and the cluster Ising (CI) chain [18],

$$H_{\text{TFI}} = - \sum_{l=1}^{L-1} \sigma_l^z \sigma_{l+1}^z + h \sum_{l=1}^L \sigma_l^x, \quad (3)$$

$$H_{\text{CI}} = - \sum_{l=1}^{L-1} \sigma_l^z \sigma_{l+1}^z - h \sum_{l=1}^{L-2} \sigma_l^x \sigma_{l+1}^x \sigma_{l+2}^z. \quad (4)$$

Both models enjoy the $\mathbb{Z}_2 \times \mathbb{Z}_2^T$ symmetry generated by $\Pi_x = \prod_{l=1}^L \sigma_l^x$ and $T = \mathcal{K}$ (the complex conjugation). There is a QCP at $h_c = 1$ in both models separating the ferromagnetic (FM) order at $|h| < h_c$ and the disorder phase at $h > h_c$. The QCPs are described by the 2D Ising CFT.

Both models are exactly solvable with the Jordan-Wigner transformation [18], $\sigma_l^z = \prod_{k=1}^{l-1} (i\gamma_k \tilde{\gamma}_k) \gamma_l$ and $\sigma_l^x = i\gamma_l \tilde{\gamma}_l$, in which the Majorana fermion operators satisfy $\{\gamma_k, \gamma_l\} = \{\tilde{\gamma}_k, \tilde{\gamma}_l\} = 2\delta_{kl}$, and $\{\gamma_k, \tilde{\gamma}_l\} = 0$. In the Majorana representation,

$$H = - \sum_{l=1}^{L-1} i\tilde{\gamma}_l \gamma_{l+1} - h \sum_{l=1}^{L-\alpha} i\tilde{\gamma}_l \gamma_{l+\alpha}, \quad (5)$$

in which $\alpha = 0$ for the TFI and 2 for the CI chain. At the QCP, both models are mapped to 1D massless Majorana fermions. However, in the CI chain, there are two decoupled Majorana modes denoted by γ_1 and $\tilde{\gamma}_L$, which lead to a two-fold degeneracy in each energy level [17, 18]. These zero modes on the edges are protected by the \mathbb{Z}_2^T symmetry [6]. In the spin representation, the degeneracy comes from the conservation of the edge spin operators $\sigma_1^z = \gamma_1$ and $\sigma_L^z = -i\tilde{\gamma}_L \Pi_x$, which mark the edge magnetization. The energy spectrum falls into four sectors

TABLE I. Scaling dimensions of the boundary spin and energy operators extracted from the connected correlation functions. Scaling dimensions in the Ising and Potts boundary CFTs are also listed for comparison.

Class	Model/b.c.	Δ_{σ}	Δ_{ϵ}
Ising	TFI	0.4992(3)	1.99957(8)
	CI	1.9984(2)	2.00008(2)
CFT	Free	1/2	2
	Fixed	2	2
Potts	Disorder-FM	0.66598(3)	0.7993(2)
	Disorder-NotA	0.6629(1)	0.7915(5)
	RSPT-FM	0.0661(3)	0.204(9)
	RSPT-NotA	0.0601(1)	0.21(1)
CFT	Free	2/3	4/5
	Dual-mixed	1/15	1/5

labeled by σ_1^z and σ_L^z . Therefore, the \mathbb{Z}_2 symmetry is spontaneously broken on the edges of the CI chain.

The connected correlation functions $C_{\perp}(L/2)$ of the spin operator σ_l^z and the energy operator $\epsilon_l = \sigma_l^z \sigma_{l+1}^z$ are used to characterize the surface critical behavior. These correlations are calculated in the Majorana representation [18] [41] (Fig. 1) and fitted to Eq. (2) with the bulk scaling dimensions $\Delta_{\sigma}^b = 1/8$ and $\Delta_{\epsilon}^b = 1$. The extracted scaling dimensions of the boundary operators are listed in Table I. While the TFI chain is captured by the Ising CFT with free b.c., the exponents of the CI chain are consistent with the fixed b.c., which can be attributed to the spontaneous edge magnetization. This property may apply to other 1D quantum critical states with degenerate edge modes as well.

The energy spectra with open boundaries are shown in Fig. 2. With proper normalization, the excitation energies map to the operator scaling dimensions, which can be compared with the operator content of the boundary CFT. The details are explained in the figure caption. Their spectra are fully consistent with the Ising CFT with free b.c. and fixed b.c., respectively.

Quantum Potts chains.—We then study the 1D generalized three-state Potts model introduced in Ref. [40]. Following their notation, the Hamiltonian is given by

$$H = H_{\text{P}} + \lambda H_0, \quad (6)$$

in which H_{P} is the simple quantum Potts model,

$$H_{\text{P}} = -J \sum_{l=1}^{L-1} (\sigma_l^{\dagger} \sigma_{l+1} + \sigma_l \sigma_{l+1}^{\dagger}) - f \sum_{l=1}^L (\tau_l + \tau_l^{\dagger}), \quad (7)$$

and H_0 is given by

$$H_0 = \sum_{l=1}^{L-1} 3((S_l^+ S_{l+1}^-)^2 - S_l^+ S_{l+1}^- + \text{H.c.}) - \sum_{l=1}^L (\tau_l + \tau_l^{\dagger}). \quad (8)$$

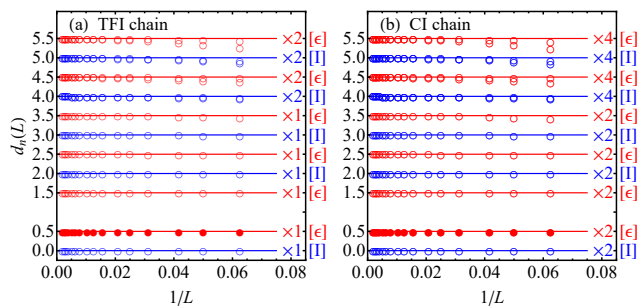


FIG. 2. Low-energy spectra of (a) the TFI and (b) the CI chains with open boundaries. The excitation energy $\Delta\epsilon_n(L) = \epsilon_n(L) - \epsilon_0(L)$ is normalized to the effective scaling dimension, $d_n(L) = \frac{1}{2} \frac{\Delta\epsilon_n(L)}{\Delta\epsilon_1(L)}$, such that the first excited state (marked with filled circles) maps to 1/2. The conformal family and the expected degeneracy in the CFT are labeled on the right. The operator content in (a) is $[\text{II}] \oplus [\epsilon]$, consistent with the Ising CFT with free b.c. [21]. In (b), the energy levels in blue come from $(\sigma_1^z, \sigma_L^z) = (+, +)$ and $(-, -)$ sectors, each forming a conformal family $[\text{II}]$, while those in red come from $(+, -)$ and $(-, +)$ sectors, each forming $[\epsilon]$. This is consistent with the fixed b.c. [21].

The operators are defined by $\tau = \text{diag}(1, \omega, \omega^2)$ with $\omega = e^{2\pi i/3}$, and

$$\sigma = \begin{pmatrix} 0 & 1 & 0 \\ 0 & 0 & 1 \\ 1 & 0 & 0 \end{pmatrix}, \quad S^+ = \begin{pmatrix} 0 & 0 & 1 \\ 1 & 0 & 0 \\ 0 & 0 & 0 \end{pmatrix} = (S^-)^\dagger. \quad (9)$$

Both terms in Eq. (6) enjoy the S_3 symmetry generated by the \mathbb{Z}_3 rotation $R = \prod_{l=1}^L \tau_l$ and the charge conjugation $C = \prod_{l=1}^L c_l$, in which

$$c = \begin{pmatrix} 1 & 0 & 0 \\ 0 & 0 & 1 \\ 0 & 1 & 0 \end{pmatrix}. \quad (10)$$

This model has a rich quantum phase diagram [40], which is sketched in Fig. 3 (a) and parametrized by $\lambda = 1 - \alpha$, $J = \alpha + \beta$, and $f = \alpha - \beta$. Besides the conventional FM Potts order characterized by the order parameter $\langle \sigma_l \rangle^3 > 0$, and the disorder phase smoothly connected to the direct product state in the $f \gg \lambda, J$ limit, there are two unconventional phases: one is the “not- A ” order with $\langle \sigma_l \rangle^3 < 0$, while the other one, dubbed the “representation SPT” (RSPT) phase, is also disordered but with a two-fold degenerate mode on each edge. A self-duality transformation reverses the sign of β , thus maps the FM to the disorder phase, and the not- A order to the RSPT phase, and vice versa. There is a continuous quantum phase transition between each order phase and each disorder phase, all of which belong to the 2D three-state Potts universality class [40]. These transition lines join at the multicritical point at $\alpha = \beta = 0$, which has

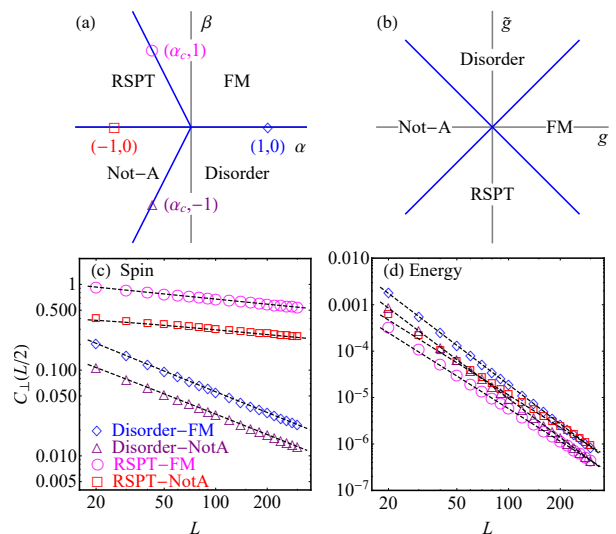


FIG. 3. (a) Schematic quantum phase diagram of the generalized Potts chain [40]. The QCPs studied in this work are marked in the figure, in which $\alpha_c = -0.50509$. (b) Global phase diagram of the effective field theory (11). Connected correlation functions $C_\perp(L/2)$ of (c) the spin operator σ_l and (d) the energy operator $\epsilon_l = \tau_l + \tau_l^\dagger$ at the QCPs. Dashed lines are the power-law fitting according to Eq. (2) plus a correction-to-scaling term, $bL^{-\Delta_\phi - \Delta_\phi^b - 1}$.

the $U(1)$ symmetry generated by $Q = \sum_l i(\tau_l - \tau_l^\dagger)$ and is described by a free boson theory. These transition lines cannot be smoothly connected without explicitly breaking the S_3 symmetry, even though they belong to the same universality class. However, unlike the CI chain, there is not any degenerate edge mode at these QCPs, thus we must find new distinctive features.

We first study the surface critical behavior. The connected correlation functions of the spin operator σ_l and the energy operator $\epsilon_l = \tau_l + \tau_l^\dagger$ are calculated with the density-matrix renormalization group (DMRG) algorithm [44–46] [41] and shown in Fig. 3. The scaling dimensions of the boundary operators are extracted by fitting Eq. (2) with $\Delta_\sigma^b = 2/15$ and $\Delta_\epsilon^b = 2$ and listed in Table I. The four QCPs fall into two classes. While the disorder-FM and the disorder-NotA transitions are captured by the Potts CFT with free b.c. [21], the RSPT-FM and the RSPT-NotA transitions yield a different set of exponents. It turns out that these exponents can be derived from the Potts CFT with the “new” conformal b.c. discovered in Refs. [42, 43]. This b.c. is S_3 symmetric and dual to the mixed b.c. [47], thus we call it the dual-mixed b.c.

In order to support the identification of these conformal b.c., we show the low-energy spectra at these QCPs with open boundaries in Fig. 4, (a–d), which are normalized to the effective scaling dimensions. The energy spectra of the disorder-FM and the disorder-NotA QCPs

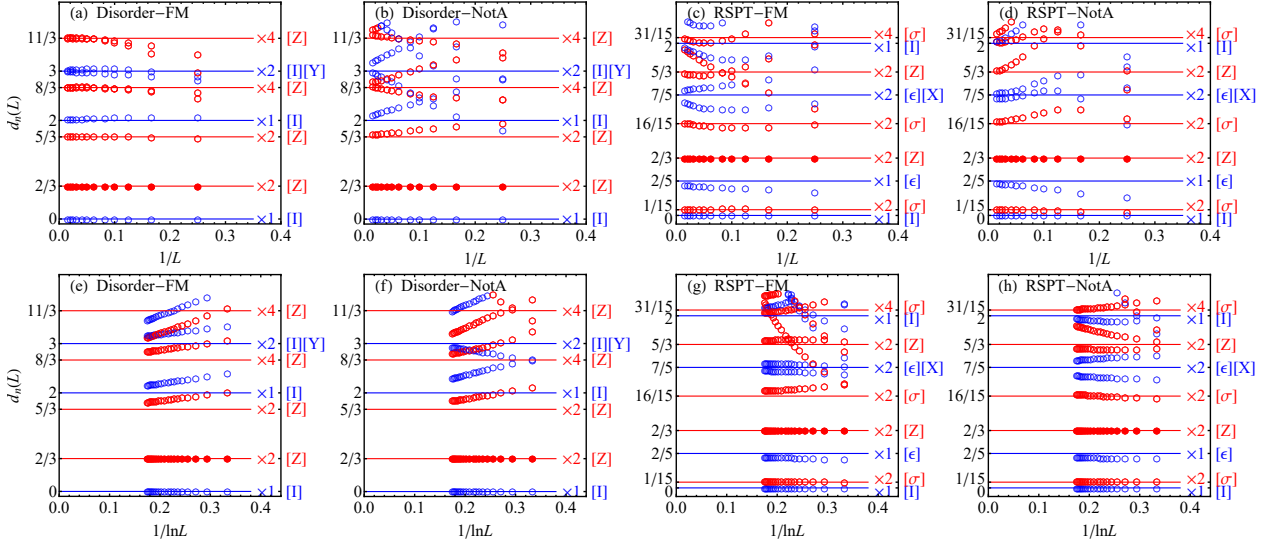


FIG. 4. (a–d) Energy spectra and (e–h) entanglement spectra of the generalized Potts chain at the QCPs. The excitation energy and the entanglement gap $\Delta\epsilon_n(L) = \epsilon_n(L) - \epsilon_0(L)$ are normalized to the effective scaling dimension, $d_n(L) = \frac{2}{3} \frac{\Delta\epsilon_n(L)}{\Delta\epsilon_Z(L)}$, such that the primary state in $[Z]$ (marked with filled circles) is normalized to $2/3$. The conformal family and the expected degeneracy in the CFT are labeled on the right. Red circles indicate numerically exact degenerate levels, while blue circles indicate non-degenerate levels. The disorder-FM and the disorder-NotA QCPs are consistent with the operator content of the Potts CFT with free b.c. $[21]$, $[\mathbb{I}] \oplus [Y] \oplus 2[Z]$, while the RSPT-FM and the RSPT-NotA QCPs are consistent with that of the dual-mixed b.c. $[42, 43]$, $[\mathbb{I}] \oplus [Y] \oplus [e] \oplus [X] \oplus 2[\sigma] \oplus 2[Z]$.

are consistent with the operator content of the Potts CFT with free b.c. On the other hand, the spectra of the RSPT-FM and the RSPT-NotA QCPs are consistent with the dual-mixed b.c.

The operator content of a boundary CFT also shows up in the bipartite entanglement spectrum of the ground state [48, 49]. The entanglement spectrum is equivalent to the energy spectrum of the CFT with a proper conformal b.c. specified at the entangling surface, i.e., the boundary between the subsystem and the rest of the chain [49]. It was found in a few 1D quantum critical states that the conformal b.c. at the entangling surface is given by the free b.c. [48], but whether other conformal b.c. can be realized at the entangling surface was not known. We calculate the entanglement spectra of the ground state at the four QCPs (Fig. 4, e–h). The entanglement spectra at the disorder-FM and the disorder-NotA QCPs are given by the operator content of the Potts CFT with free b.c., which confirms the observation in Ref. [48]. However, we find that the entanglement spectra at the RSPT-FM and the RSPT-NotA QCPs are drastically different and consistent with the Potts CFT with dual-mixed b.c. instead. Therefore, the distinct conformal b.c. is realized at both the physical and the entangling surfaces.

We now argue that these distinct conformal b.c. can be derived from the bulk effective field theory proposed in Ref. [40]. The global quantum phase diagram is captured by the following self-dual sine-Gordon theory with the

Hamiltonian density [see Fig. 3 (b)],

$$\mathcal{H} = \frac{1}{2}(\partial_x\phi)^2 + \frac{1}{2}(\partial_x\theta)^2 - g\cos(3\phi) - \tilde{g}\cos(3\theta), \quad (11)$$

in which ϕ and θ are the scalar field and the dual disorder field, respectively. The $U(1)$ -symmetric multicritical point is captured by the free boson theory at $g = \tilde{g} = 0$. The g and \tilde{g} terms are relevant at the multicritical point. For $g > |\tilde{g}| > 0$, ϕ is polarized to 0 or $\pm 2\pi/3$ and gives the FM order, while for $g < -|\tilde{g}| < 0$, ϕ is polarized to π or $\pm\pi/3$, i.e., an equal-weight superposition of two out of the three spin states, and describes the not- A order. For $\tilde{g} > |g| > 0$, the disorder field θ is pinned at 0 or $\pm 2\pi/3$, while for $\tilde{g} < -|g| < 0$, θ is pinned at π or $\pm\pi/3$. From the duality relation, the former corresponds to the disorder phase, while the latter is the RSPT phase. The transition lines are given by $|g| = |\tilde{g}|$.

Given that the disorder-FM transition at $g = \tilde{g} > 0$ realizes the free b.c. [21], the dual field θ is pinned at 0 or $\pm 2\pi/3$ at the boundary due to the duality between the free b.c. and the fixed b.c. [50]. At the RSPT-FM transition for $\tilde{g} = -g < 0$, the sign of \tilde{g} is reversed, thus θ is pinned at π or $\pm\pi/3$ at the boundary, corresponding to the mixed b.c. of the θ field and thus the dual-mixed b.c. in terms of the ϕ field. On the other hand, the conformal b.c. is not changed by reversing the sign of g , because the ϕ field is not polarized at the boundary of any of these QCPs. Therefore, the disorder-NotA transition at $g = -\tilde{g} < 0$ realizes the free b.c., while the RSPT-NotA

transition at $g = \tilde{g} < 0$ shows the dual-mixed b.c. These arguments are consistent with our numerical results, and thereby establish a novel bulk-boundary correspondence between the bulk effective field theory and the conformal b.c. of the symmetry-enriched quantum critical states.

Conclusion.—To summarize, we have studied the surface critical behavior and the conformal b.c. of 1D generalized Ising and Potts models. In each family, we focused on the quantum critical states that cannot be smoothly connected without explicitly breaking certain symmetries even though they are captured by the same CFT. The degenerate edge modes of the critical CI chain spontaneously break the \mathbb{Z}_2 symmetry and lead to the fixed b.c. of the Ising CFT. On the other hand, the QCPs of the RSPT phase in the generalized Potts chain, which do not have any degenerate edge modes, realize the dual-mixed b.c. of the Potts CFT, in sharp contrast to the free b.c. of the simple quantum Potts chain. Therefore, the conformal b.c. is a more generic characteristic of symmetry-enriched quantum critical states beyond the edge degeneracy. Moreover, we argued that the conformal b.c. can be derived from the effective field theory of the bulk states, thus established a novel bulk-boundary correspondence in these quantum critical systems.

We thank Paul Fendley, Shang Liu, Rong-Yang Sun, Huajia Wang, and Yijian Zou for helpful discussions and communications. Part of the numerical simulations was carried out with the ITensor package [51]. L.Z. is supported by the National Key R&D Program of China (2018YFA0305800), the National Natural Science Foundation of China (11804337 and 12174387), the Strategic Priority Research Program of CAS (XDB28000000), and the CAS Youth Innovation Promotion Association. X.-J.Y. and L.X. is supported by National Natural Science Foundation of China under Grant No. 11935002, the National Key R&D Program under Grant No. 2016YFA0300901. R.-Z.H. is supported by China Postdoctoral Science Foundation (Grant No. 2020T130643), the Fundamental Research Funds for the Central Universities and the National Natural Science Foundation of China (Grants No. 12047554). C.D. is supported by the National Natural Science Foundation of China (11975024 and 11774002), and Anhui Provincial Supporting Program for Excellent Young Talents in Colleges and Universities (gxyqZD2019023).

* These authors contributed equally.

† longzhang@ucas.ac.cn

- [1] X.-G. Wen, *Rev. Mod. Phys.* **89**, 041004 (2017).
 [2] Z.-C. Gu and X.-G. Wen, *Phys. Rev. B* **80**, 155131 (2009).
 [3] F. Pollmann, A. M. Turner, E. Berg, and M. Oshikawa, *Phys. Rev. B* **81**, 064439 (2010).
 [4] A. Keselman and E. Berg, *Phys. Rev. B* **91**, 235309

- (2015).
 [5] T. Scaffidi, D. E. Parker, and R. Vasseur, *Phys. Rev. X* **7**, 041048 (2017).
 [6] R. Verresen, R. Thorngren, N. G. Jones, and F. Pollmann, arXiv:1905.06969.
 [7] M. Cheng and H.-H. Tu, *Phys. Rev. B* **84**, 094503 (2011).
 [8] L. Fidkowski, R. M. Lutchyn, C. Nayak, and M. P. Fisher, *Phys. Rev. B* **84**, 195436 (2011).
 [9] J. D. Sau, B. I. Halperin, K. Flensberg, and S. Das Sarma, *Phys. Rev. B* **84**, 144509 (2011).
 [10] J. P. Kestner, B. Wang, J. D. Sau, and S. Das Sarma, *Phys. Rev. B* **83**, 174409 (2011).
 [11] F. Iemini, L. Mazza, D. Rossini, R. Fazio, and S. Diehl, *Phys. Rev. Lett.* **115**, 156402 (2015).
 [12] N. Lang and H. P. Büchler, *Phys. Rev. B* **92**, 041118 (2015).
 [13] J. Ruhman and E. Altman, *Phys. Rev. B* **96**, 085133 (2017).
 [14] H.-C. Jiang, Z.-X. Li, A. Seidel, and D.-H. Lee, *Sci. Bull.* **63**, 753 (2018).
 [15] D. E. Parker, T. Scaffidi, and R. Vasseur, *Phys. Rev. B* **97**, 165114 (2018).
 [16] A. Keselman, E. Berg, and P. Azaria, *Phys. Rev. B* **98**, 214501 (2018).
 [17] R. Verresen, N. G. Jones, and F. Pollmann, *Phys. Rev. Lett.* **120**, 057001 (2018).
 [18] N. G. Jones and R. Verresen, *J. Stat. Phys.* **175**, 1164 (2019).
 [19] R. Verresen, arXiv:2003.05453.
 [20] R. Thorngren, A. Vishwanath, and R. Verresen, *Phys. Rev. B* **104**, 075132 (2021).
 [21] J. L. Cardy, *Nucl. Phys. B* **275**, 200 (1986).
 [22] J. L. Cardy, *Nucl. Phys. B* **324**, 581 (1989).
 [23] J. L. Cardy, *Nucl. Phys. B* **240**, 514 (1984).
 [24] K. Binder, in *Phase Transitions and Critical Phenomena*, Vol. 8, edited by C. Domb and J. L. Lebowitz (Academic Press, London, England, 1983).
 [25] H. W. Diehl, in *Phase Transitions and Critical Phenomena*, Vol. 10, edited by C. Domb and J. L. Lebowitz (Academic Press, London, 1986).
 [26] T. Grover and A. Vishwanath, arXiv:1206.1332.
 [27] T. Suzuki and M. Sato, *Phys. Rev. B* **86**, 224411 (2012).
 [28] L. Zhang and F. Wang, *Phys. Rev. Lett.* **118**, 087201 (2017).
 [29] C. Ding, L. Zhang, and W. Guo, *Phys. Rev. Lett.* **120**, 235701 (2018).
 [30] L. Weber, F. Parisen Toldin, and S. Wessel, *Phys. Rev. B* **98**, 140403 (2018).
 [31] L. Weber and S. Wessel, *Phys. Rev. B* **100**, 054437 (2019).
 [32] L. Weber and S. Wessel, *Phys. Rev. B* **103**, L020406 (2021).
 [33] W. Zhu, C. Ding, L. Zhang, and W. Guo, *Phys. Rev. B* **103**, 024412 (2021).
 [34] C. Ding, W. Zhu, W. Guo, and L. Zhang, arXiv:2110.04762.
 [35] F. Parisen Toldin, *Phys. Rev. Lett.* **126**, 135701 (2021).
 [36] M. Hu, Y. Deng, and J.-P. Lv, *Phys. Rev. Lett.* **127**, 120603 (2021).
 [37] F. Parisen Toldin and M. A. Metlitski, arXiv:2111.03613.
 [38] C.-M. Jian, Y. Xu, X.-C. Wu, and C. Xu, *SciPost Phys.* **10**, 033 (2021).
 [39] M. A. Metlitski, arXiv:2009.05119.
 [40] E. O'Brien, E. Vernier, and P. Fendley, *Phys. Rev. B*

- 101**, 235108 (2020).
- [41] See the Supplemental Materials, which also include Refs. [52–57].
- [42] I. Affleck, M. Oshikawa, and H. Saleur, *J. Phys. A* **31**, 5827 (1998).
- [43] J. Fuchs and C. Schweigert, *Phys. Lett. B* **441**, 141 (1998).
- [44] S. R. White, *Phys. Rev. Lett.* **69**, 2863 (1992).
- [45] U. Schollwöck, *Rev. Mod. Phys.* **77**, 259 (2005).
- [46] U. Schollwöck, *Ann. Phys. (N. Y.)* **326**, 96 (2011).
- [47] With the mixed b.c., the edge spin is polarized as an equal-weight superposition of two out of the three spin states with the edge order $\langle \sigma \rangle^3 < 0$.
- [48] A. M. Läuchli, arXiv:1303.0741.
- [49] J. Cardy and E. Tonni, *J. Stat. Mech.* **2016**, 123103 (2016).
- [50] K. Drühl and H. Wagner, *Ann. Phys. (N. Y.)* **141**, 225 (1982).
- [51] M. Fishman, S. R. White, and E. M. Stoudenmire, arXiv:2007.14822.
- [52] F. Verstraete, V. Murg, and J. Cirac, *Adv. Phys.* **57**, 143 (2008).
- [53] F. Verstraete and J. I. Cirac, *Phys. Rev. B* **73**, 094423 (2006).
- [54] J. Haegeman and F. Verstraete, *Annu. Rev. Condens. Matter Phys.* **8**, 355 (2017).
- [55] V. Zauner-Stauber, L. Vanderstraeten, M. T. Fishman, F. Verstraete, and J. Haegeman, *Phys. Rev. B* **97**, 045145 (2018).
- [56] M. Rader and A. M. Läuchli, *Phys. Rev. X* **8**, 031030 (2018).
- [57] P. Corboz, P. Czarnik, G. Kapteijns, and L. Tagliacozzo, *Phys. Rev. X* **8**, 031031 (2018).

Conformal Boundary Conditions of Symmetry-Enriched Quantum Critical Spin Chains: Supplemental Materials

Xue-Jia Yu,^{1,*} Rui-Zhen Huang,^{2,*} Hong-Hao Song,²
Limei Xu,^{1,3,4} Chengxiang Ding,⁵ and Long Zhang^{2,†}

¹*International Center for Quantum Materials,
School of Physics, Peking University, Beijing 100871, China*

²*Kavli Institute for Theoretical Sciences and CAS Center
for Excellence in Topological Quantum Computation,
University of Chinese Academy of Sciences, Beijing, 100190, China*

³*Collaborative Innovation Center of Quantum Matter, Beijing, China*

⁴*Interdisciplinary Institute of Light-Element Quantum Materials and Research
Center for Light-Element Advanced Materials, Peking University, Beijing, China*

⁵*School of Science and Engineering of Mathematics and Physics,
Anhui University of Technology, Maanshan, Anhui 243002, China*

(Dated: November 23, 2021)

Abstract

In these appendices, we show the calculation details on the correlation functions of the generalized Ising chains, and the quantum critical point and the correlation functions of the generalized three-state Potts chain.

I. CORRELATION FUNCTIONS OF THE GENERALIZED ISING CHAINS

The TFI and the CI chains can be mapped to free Majorana fermions with the Jordan-Wigner transformation¹, $\sigma_l^z = \prod_{k=1}^{l-1} (i\gamma_k \tilde{\gamma}_k) \gamma_l$ and $\sigma_l^x = i\gamma_l \tilde{\gamma}_l$, in which the Majorana fermion operators satisfy $\{\gamma_k, \gamma_l\} = \{\tilde{\gamma}_k, \tilde{\gamma}_l\} = 2\delta_{kl}$, and $\{\gamma_k, \tilde{\gamma}_l\} = 0$. In the Majorana representation,

$$H = - \sum_{l=1}^{L-1} i\tilde{\gamma}_l \gamma_{l+1} - h \sum_{l=1}^{L-\alpha} i\tilde{\gamma}_l \gamma_{l+\alpha}, \quad (1)$$

in which $\alpha = 0$ for the TFI and 2 for the CI chain. At the quantum critical point (QCP), both models are mapped to 1D massless Majorana fermions.

In order to diagonalize the Hamiltonian (1), we first rewrite it with complex fermion operators c_l and c_l^\dagger : $\gamma_l = c_l^\dagger + c_l$ and $\tilde{\gamma}_l = i(c_l^\dagger - c_l)$,

$$H = \sum_{i,j} \left(c_i^\dagger A_{ij} c_j + \frac{1}{2} (c_i^\dagger B_{ij} c_j^\dagger + \text{H.c.}) \right), \quad (2)$$

in which the matrix A is Hermitian, and B is antisymmetric. We then perform the canonical transformation,

$$\eta_k = \sum_i (g_{ki} c_i + h_{ki} c_i^\dagger), \quad (3)$$

$$\eta_k^\dagger = \sum_i (g_{ki} c_i^\dagger + h_{ki} c_i), \quad (4)$$

in which g_{ki} and h_{ki} satisfy the orthogonality conditions,

$$\sum_i (g_{ki} g_{li} + h_{ki} h_{li}) = \delta_{kl}, \quad (5)$$

$$\sum_i (g_{ki} h_{li} + h_{ki} g_{li}) = 0, \quad (6)$$

and the secular equations,

$$\sum_i (g_{ki} A_{il} - h_{ki} B_{il}) = \Lambda_k g_{kl}, \quad (7)$$

$$\sum_i (g_{ki} B_{il} - h_{ki} A_{il}) = \Lambda_k h_{kl}. \quad (8)$$

The Hamiltonian is diagonalized,

$$H = \sum_k \Lambda_k \eta_k^\dagger \eta_k, \quad (9)$$

in which the eigenstate energy $\Lambda_k \geq 0$, thus the ground state corresponds to the vacuum state of the complex fermions η_k 's.

The equal-time spin correlation function at the ground state is given by

$$\langle \sigma_l^z \sigma_m^z \rangle = \left\langle \prod_{i=l}^{m-1} (i\tilde{\gamma}_i \gamma_{i+1}) \right\rangle, \quad l < m. \quad (10)$$

According to the Wick theorem, the correlation function of mutually anticommuting operators \mathcal{A}_i 's is given by

$$\langle \mathcal{A}_1 \cdots \mathcal{A}_{2n} \rangle = \sum_{\text{all pairings}} (-1)^\sigma \prod_{\text{all pairs } (ij)} \langle \mathcal{A}_i \mathcal{A}_j \rangle, \quad (11)$$

in which $(-1)^\sigma$ is the parity of the permutation. Define $\phi_{ki} = g_{ki} + h_{ki}$, $\psi_{ki} = g_{ki} - h_{ki}$, then the pair correlations of Majorana operators are given by

$$\langle \gamma_i \gamma_j \rangle = \sum_k \phi_{ki} \phi_{kj} = \delta_{ij}, \quad (12)$$

$$\langle \tilde{\gamma}_i \tilde{\gamma}_j \rangle = \sum_k \psi_{ki} \psi_{kj} = \delta_{ij}, \quad (13)$$

$$\langle i\tilde{\gamma}_i \gamma_j \rangle = \sum_k \psi_{ki} \phi_{kj} \equiv G_{ij}. \quad (14)$$

Therefore, we find

$$\langle \sigma_l^z \sigma_m^z \rangle = \begin{vmatrix} G_{l,l+1} & G_{l,l+2} & \cdots & G_{l,m} \\ G_{l+1,l+1} & G_{l+1,l+2} & \cdots & G_{l+1,m} \\ \vdots & \vdots & \ddots & \vdots \\ G_{m-1,l+1} & G_{m-1,l+2} & \cdots & G_{m-1,m} \end{vmatrix}. \quad (15)$$

For the TFI chain, the connected correlation function of the spin operator σ_l^z is given by

$$C_\perp(1, 1 + L/2) = \langle \sigma_1^z \sigma_{1+L/2}^z \rangle. \quad (16)$$

For the CI chain, the ground state is two-fold degenerate due to the spontaneous magnetization on the edges. We take the expectation value over an eigenstate of σ_1^z , then $\langle \sigma_1^z \sigma_l^z \rangle = \langle \sigma_1^z \rangle \langle \sigma_l^z \rangle$, thus the connected correlation $C_\perp(1, r) = \langle \sigma_1^z \sigma_r^z \rangle_c = 0$. Therefore, we calculate the connected correlation function of the second site with the bulk instead,

$$C_\perp(2, 2 + L/2) = \langle \sigma_2^z \sigma_{2+L/2}^z \rangle - \langle \sigma_2^z \rangle \langle \sigma_{2+L/2}^z \rangle = \langle \sigma_2^z \sigma_{2+L/2}^z \rangle - \langle \sigma_1^z \sigma_2^z \rangle \langle \sigma_1^z \sigma_{2+L/2}^z \rangle. \quad (17)$$

The connected correlation function of the energy operator $\epsilon_l = \sigma_l^z \sigma_{l+1}^z$ is also calculated in the Majorana representation,

$$C_\perp(L/2) = \langle \epsilon_1 \epsilon_{1+L/2} \rangle - \langle \epsilon_1 \rangle \langle \epsilon_{1+L/2} \rangle = \langle i\tilde{\gamma}_1 \gamma_{2+L/2} \rangle \langle i\tilde{\gamma}_2 \tilde{\gamma}_{1+L/2} \rangle. \quad (18)$$

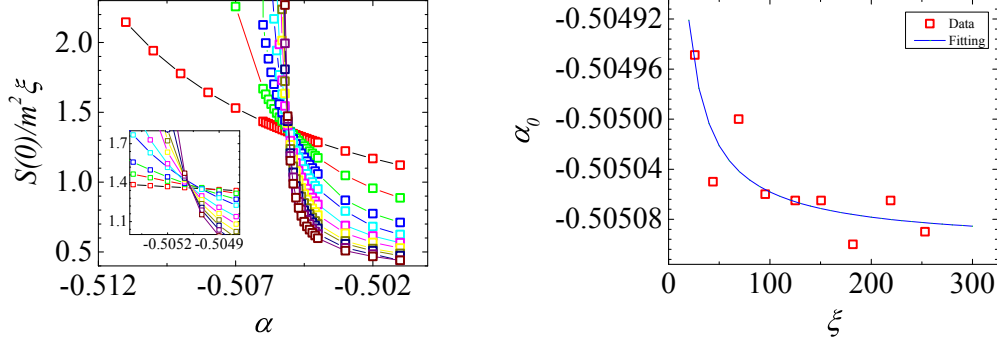


FIG. 1: The crossing points of the dimensionless quantity $\frac{S(0)}{m^2\xi}$ calculated with different bond dimension D (left panel) provide estimate of the critical point α_c , which is extrapolated to the infinite- ξ limit with $\alpha_c(\xi) = \alpha_c + b\xi^{-\omega}$ (right panel).

II. NUMERICAL SIMULATION OF THE GENERALIZED POTTS CHAIN

We apply the matrix product state (MPS) based numerical methods^{2,3} to calculate the quantum critical behavior of the generalized Potts chain. The MPS is a class of wavefunctions constructed as the product of a set of $D \times D$ matrices at each site, in which D is called the bond dimension. They represent low-entanglement quantum many-body states faithfully and are the underlying wavefunctions of the density matrix renormalization group (DMRG) algorithm⁴. MPS can accurately describe the low-energy properties of one-dimensional (1D) gapped systems^{5,6}, while for critical systems, MPS can be adopted for finite-size scaling analysis.

A. Bulk quantum critical point

We use the variational uniform infinite MPS^{7,8} to determine the RSPT-FM QCP of the generalized three-state Potts chain. The uniform infinite MPS is translationally invariant and defined directly in the thermodynamic limit. For a given uniform infinite MPS with a bond dimension D , the correlation length ξ is defined by

$$\xi^{-1} = \ln(\lambda_0/\lambda_1), \quad (19)$$

in which λ_0 and λ_1 are the largest two eigenvalues of the transfer matrix constructed with the local MPS tensor^{7,8}.

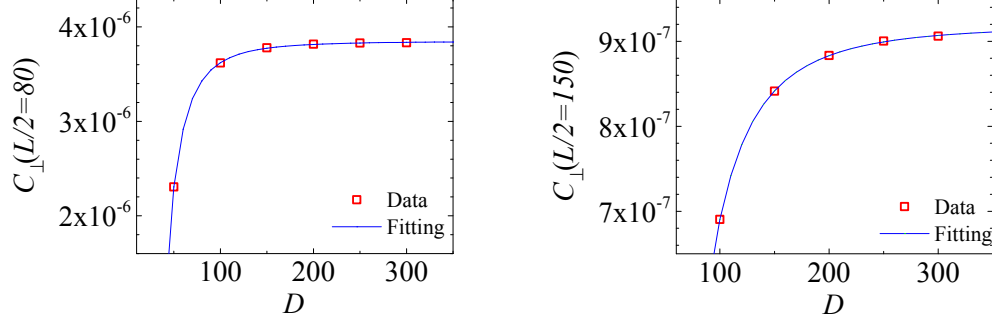


FIG. 2: Examples of finite- D scaling of the energy correlation function $C_{\perp}(L/2)$ at the QCP of the generalized Potts chain. The data converge to the infinite- D limit exponentially, and are fitted with $c + ae^{-bD}$.

We fix $\beta = 1$, and calculate the approximate ground states for different α with various bond dimensions D . The largest D used in the simulation is 300. Several random initial states are used to avoid local minima. The structure factor of the order parameter is defined by

$$S(q) = \sum_i e^{iqr_i} \langle \sigma_0 \sigma_i \rangle_c, \quad (20)$$

in which the infinite sum can be efficiently calculated with the pseudo-inverse of the transfer matrix^{7,8}. Near the RSPT-FM QCP, $S(0)$ has the same scaling dimension as $m^2\xi$, in which m is the order parameter. The following dimensionless ratio has the scaling form^{9,10},

$$\frac{S(0)}{m^2\xi} = f(g\xi^{1/\nu}), \quad (21)$$

in which $g = \alpha - \alpha_c$. As shown in Fig. 1, the crossing point of this ratio calculated with different D give the estimate of the critical point α_c . By extrapolating to the infinite- ξ limit, we find $\alpha_c = -0.50509(4)$ for $\beta = 1$. The disorder-NotA QCP is obtained by the self-duality mapping as $(\alpha_c, -1)$.

B. Boundary correlation functions

We use the DMRG algorithm⁴ on finite lattices to calculate the correlation functions of the generalized Potts chain with open boundary condition at the QCPs. For various bond dimensions D , we carry out two-site DMRG calculations followed by single-site DMRG sweeps until convergence to achieve the accurate ground state wavefunctions. The correlation

functions are calculated for these MPS wavefunctions, and then extrapolated to the infinite- D limit (see Fig. 2). These extrapolated correlations are then fed into the finite-size scaling analysis in the main text.

* These authors contributed equally.

† Electronic address: longzhang@ucas.ac.cn

- ¹ N. G. Jones and R. Verresen, *J. Stat. Phys.* **175**, 1164 (2019).
- ² F. Verstraete, V. Murg, and J. Cirac, *Adv. Phys.* **57**, 143 (2008).
- ³ U. Schollwöck, *Ann. Phys. (N. Y.)* **326**, 96 (2011).
- ⁴ S. R. White, *Phys. Rev. Lett.* **69**, 2863 (1992).
- ⁵ U. Schollwöck, *Rev. Mod. Phys.* **77**, 259 (2005).
- ⁶ F. Verstraete and J. I. Cirac, *Phys. Rev. B* **73**, 094423 (2006).
- ⁷ J. Haegeman and F. Verstraete, *Annu. Rev. Condens. Matter Phys.* **8**, 355 (2017).
- ⁸ V. Zauner-Stauber, L. Vanderstraeten, M. T. Fishman, F. Verstraete, and J. Haegeman, *Phys. Rev. B* **97**, 045145 (2018).
- ⁹ M. Rader and A. M. Läuchli, *Phys. Rev. X* **8**, 031030 (2018).
- ¹⁰ P. Corboz, P. Czarnik, G. Kapteijns, and L. Tagliacozzo, *Phys. Rev. X* **8**, 031031 (2018).